Small Molecules Target the Interaction between Tissue Transglutaminase and Fibronectin

Livia Elena Sima[#,1], **Bakhtiyor Yakubov**[#,2], **Sheng Zhang**[3], **Salvatore Condello**[1], **Arabela A. Grigorescu**[4], **Nkechiyere G. Nwani**[1], **Lan Chen**[3], **Gary E. Schiltz**[5,6,7], **Constandina Arvanitis**[8], **Zhong-Yin Zhang**[3], and **Daniela Matei**[1,7,9]

[1]Department of Obstetrics and Gynecology, Feinberg School of Medicine, Northwestern University, Chicago, IL 60611, USA

[2]Department of Medicine, Indiana University School of Medicine, Indianapolis, IN, USA

[3]Department of Medicinal Chemistry and Molecular Pharmacology and Institute for Drug Discovery, Purdue University, IN, USA

[4]Keck Biophysics Facility, Northwestern University, Evanston, IL, USA

[5]Center for Molecular Innovation and Drug Discovery, Northwestern University, Evanston, Illinois, 60208, USA

[6]Department of Pharmacology, Northwestern University, Chicago, 60611, Illinois, USA

[7]Robert H. Lurie Comprehensive Cancer Center, Feinberg School of Medicine, Northwestern University, Chicago, 60611, Illinois, USA

[8]Center for Advanced Microscopy and Department of Cell and Molecular Biology, Northwestern University Feinberg School of Medicine, Chicago, IL, USA

[9]Jesse Brown VA Medical Center, Chicago, IL

Abstract

Tissue transglutaminase (TG2) is a multi-functional protein, with enzymatic, GTP-ase and scaffold properties. TG2 interacts with fibronectin (FN) through its N-terminus domain, stabilizing integrin complexes, which regulate cell adhesion to the matrix. Through this mechanism, TG2 participates in key steps involved in metastasis in ovarian and other cancers. High throughput screening identified several small molecule inhibitors (SMIs) for the TG2/FN complex. Rational medicinal chemistry optimization of the hit compound (TG53) led to second generation analogues (MT1–6). ELISA demonstrated that these analogues blocked TG2/FN interaction and bio-layer interferometry (BLI) showed that the SMIs bound to TG2. The compounds also potently inhibited cancer cell adhesion to FN and decreased outside-in signaling mediated through the focal adhesion kinase (FAK). Blockade of TG2/FN interaction by the small molecules caused membrane ruffling, delaying the formation of stable focal contacts and mature adhesions points and disrupted

Corresponding Author: Daniela Matei, MD, Professor, Department of Obstetrics and Gynecology, Northwestern University Feinberg School of Medicine, 303 E Superior Street, Lurie 4-107, Tel: 312-472-4065, daniela.matei@northwestern.edu.
[#]These authors contributed equally

Conflict of Interest: The authors declare no potential conflicts of interest.

organization of the actin cytoskeleton. In an *in vivo* model measuring intraperitoneal (ip) dissemination, MT4 and MT6 inhibited the adhesion of ovarian cancer (OC) cells to the peritoneum. Pre-treatment with MT4 also sensitized OC cells to paclitaxel. The data support continued optimization of the new class of SMIs that block the TG2/FN complex at the interface between cancer cells and the tumor niche.

Keywords

small molecule inhibitors; tissue transglutaminase; fibronectin; integrin β1; ovarian cancer

Introduction:

Interactions between cancer cells and the tumor niche occur early during tumorigenesis and promote cell survival, evasion from chemotherapy, and establishment of metastatic sites. In ovarian cancer (OC), contact with the fibronectin (FN) and collagen-rich mesothelial matrix critically regulates the steps of peritoneal dissemination(1). We identified tissue transglutaminase (TG2), a protein which anchors epithelial cells into the extracellular matrix (ECM) through interactions with FN and integrins(2), as being highly expressed in ovarian tumors at the interface between cancer cells and the tumor microenvironment (TME) (3). We showed that when injected intraperitoneally (ip) or under the ovarian bursa of nude mice, OC cells engineered to express decreased levels of *TG2* disseminated less efficiently, as compared to control cells(3–5).

The process of metastasis in solid tumors requires loss of cell-cell contact and breakdown of the basement membrane followed by tumor invasion into lymphatic or vascular channels(6). By contrast, OC harbors a distinct pattern of peritoneal metastasis, with hematogenous dissemination being uncommon(1). OC cells are in direct contact with the overlying peritoneal surface and fluid and simple dislodgement from the primary tumor allows cells to float in the peritoneal space, where they adhere and form metastatic implants. In the peritoneal fluid, OC cells aggregate as spheroids, which provide protection from the stress imposed by the extracellular environment. Interactions between cancer cells and the peritoneal mesothelium activate "outside-in" signaling (7) which stimulates cell proliferation, survival and tumor angiogenesis. Over the past decade, our group demonstrated sequentially that TG2 regulates EMT (4), migration of cells from the primary site(3), formation of spheroids in the peritoneal fluid (8), and invasion into the peritoneum (3, 9). These steps regulated by the protein through its interaction with FN contribute to establishment of peritoneal implants (3, 4) and render TG2 an attractive new cancer target.

TG2 is a multifunctional protein, which catalyzes Ca^{2+}-dependent post-translational protein modifications and has a well-defined binding site for FN. Our mechanistic studies identified the interaction between TG2 and FN as being a critical player in the process of intraperitoneal (ip) dissemination. We demonstrated that the TG2/FN complex is implicated in OC metastasis via multiple mechanisms including: adhesion to the ECM by strengthening integrin-dependent cell-matrix adhesion (3), induction of epithelial to mesenchymal transition (EMT) (4, 8), regulation of Wnt/β-catenin signaling (10), through direct

interaction with the Frizzled 7 (Fzd7) receptor, which in turn drives OC cell proliferation and persistence of a stem cell profile (5), remodeling of the extracellular matrix (11), and fine tuning of intracellular oncogenic signaling (10, 12). An antibody that disrupted TG2/FN complexes inhibited cancer stemness characteristics, spheroid formation, and tumor initiation (5).

Based on these results, we hypothesized that the TG2/FN interaction is targetable and that its disruption by small molecules will prevent cancer cell adhesion to the matrix and OC metastasis. To this end, we completed a high throughput screening (HTS) campaign of compounds in the ChemDiv library by using a newly developed AlphaLISA assay that robustly measured the TG2/FN complex formation and identified a new class of potent inhibitors for this protein-protein interaction (PPI) (13). We showed that several of the small molecules discovered through the screen potently blocked OC cell adhesion and migration, demonstrating proof-of-principle for blocking this protein complex to diminish cancer cell invasiveness and perhaps peritoneal dissemination. The best hit (TG53) exhibited good biochemical potency and had highly efficacious cellular activity. Given its promising properties, we used TG53 as a starting point to develop more potent and selective TG2/FN inhibitors by using rational medicinal chemistry optimization. Here we show that newly synthesized analogues possess improved *in vitro* and *in vivo* efficacy in OC models. This new series of TG2/FN inhibitors potently blocks cellular adhesion to FN and to a reconstituted peritoneal matrix, resulting in inhibition of "outside-in" signaling and sensitization of cancer cells to paclitaxel. Our results identify new small molecules targeting the TG2/FN complex and the initial steps of cellular adhesion for future preclinical development.

Materials and Methods

Chemicals and reagents

Unless stated otherwise, chemicals and reagents were from Sigma-Aldrich (St Louis, MO, USA). Anti-integrin β1 antibody was from Chemicon (Cambridge, MA, USA); PE anti-CD29/integrin β1 (#303004), from BioLegend (San Diego, CA, USA); anti-pERK1/2(# 9101), anti-ERK (# 9102), anti-pFAK (#3283), and anti-FAK (#3285), from Cell Signaling (Beverly, MA, USA); anti-vinculin (#ab18058), from Abcam(Cambridge, MA, USA); anti-pFAK(#44–625G)used for IF was from Thermo Scientific (Fremont, CA, USA);and anti-GAPDH from Biodesign International (Saco, ME, USA). Antibodies for phospho-Src (Tyr416), phospho-FAK (Tyr576/577), and c-Src used for confocal imaging were from Cell Signaling Technology, Inc. (Beverly, MA, USA), monoclonal TG2 (CUB 7402) was from Thermo Fisher Scientific, integrin β1 was from EMD Millipore (Billerica, MA, USA).Secondary HRP-conjugated antibodies were from Amersham Biosciences (San Francisco, CA, USA) and Santa Cruz Biotechnology Inc (Santa Cruz, CA, USA).

Cell culture

SKOV3 cells were obtained from the American Type Culture Collection (ATCC, Manassas, VA), and cultured in growth media containing 1:1 MCDB 105 (Sigma, St. Louis, MO) and M199 (Cellgro, Manassas, VA).OVCAR5. SKOV3-GFP, and OVCAR433 were provided by

Drs. Peter (Northwestern University, Chicago, IL) and Bigbsy (Indiana University, Indianapolis, IN), respectively, and were grown in RPMI media (Corning). LP9, a mesothelial cell line, was procured from the Coriell Institute (Camden, New Jersey, USA) and grown in M199/MCDB 151 medium with 15% FBS and 0.4 µg/ml hydrocortisone. Media was supplemented with 10% FBS and 1% Penicillin-Streptomycin. Cells were cultured at 37°C in a humidified incubator with 5% CO2. All cells were authenticated and tested negative for Mycoplasma at least yearly. Cells were passaged no more than 15 times after thawing.

Design and synthesis of TG-53 analogues.

The synthetic schemes and detailed experimental procedures are included in Supplemental Information. All six compounds **MT**-**1–6** were synthesized from a common intermediate N2-(4-aminophenyl)-N4,N4,6-trimethylpyrimidine-2,4-diamine (compound **S1**, structure shown in Supplemental Material). Compound **S1** was prepared from commercially available compounds crimidine and *p*-phenylenediamine. A solution of crimidine and *p*-phenylenediamine (1:1 mole ratio) in dimethyl formamide (DMF), were sealed in a glass microwave reactor and radiated with microwave to heat up to 150 °C and maintained for 15 min. After cooling to room temperature, the solid product was collected by filtration, and washed with ethyl acetate to give compound **S1**. Compound **S1** was then condensed with different carboxylic acids in DMF, using propyl phosphonic anhydride (T3P) as the coupling reagent to give the desired products (**MT-1–6**). Compounds were purified by reversed-phase HPLC and purity was confirmed with LC-MS and NMR (Figures S1–S6).

Bio-layer Interferometry (BLI) and Isothermal Titration Calorimetry (ITC)

The 45kDa fibronectin fragment (FN45) corresponding to the TG2 binding region (Sigma, #F0162) was biotinylated using Biotin (Type A) Fast Conjugation Kit (Abcam, #ab201795). Biotinylated FN45 (10 µg/mL in PBS) was captured on pre-hydrated streptavidin-coated sensors (Pall Forte Bio SAX 18–5117). At each TG2 concentration, the binding kinetics were determined by following this sequence run: baseline (PBS for 30s), association step (varying concentrations of TG2 in PBS for 120s), and dissociation step (PBS for 120s). A new FN45 biosensor was prepared for each run. To analyze the effect of the inhibitor MT4 on the interaction between TG2 and FN, a solution of 20µg/mL of bio-FN45 was used for capturing FN45 on the streptavidin-coated sensors and the association step was 90s. For each sensor, the capturing step was measured in real-time in order to assess the stability of the signal and the reproducibility between sensors. The saturation level Rmax was 0. 6 (±0.08) for all sensors and no dissociation of the biotinylated FN45 was observed over 60 minutes. Control experiments performed with bare sensors (without FN45) showed no significant binding of TG2. For the experiments with (TG2 + MT4), controls were performed at each MT4 concentration and Rmax values were corrected for non-specific binding and any effects of DMSO on the TG2-FN45 interaction (these effects were below 8%). All BLI experiments were performed at 22° C. Data fitted globally using the BLItz Pro 1.10.31 software package as described(14, 15). Isothermal titration calorimetry (ITC) was performed at 25 °C by titrating160 µM MT4 into a 10 µM solution of TG2 (Sigma, #T5398).

Cell adhesion to LP9 mesothelial cells monolayers

LP9 mesothelial cells added to clear-bottom 96-well plate at 12,000 cells/well were grown to confluency over 48 hours (h). OC cells were labeled with calcein AM and seeded at a density of 4×10^4 cells to monolayers of mesothelial cells and incubated for 1h. Non-adherent cells were removed by washing with PBS.

Total internal reflection fluorescence (TIRF) microscopy

For assessing the potential effect of SMIs on β1 integrin distribution at the interface between cells and the FN matrix, OVCAR5 cells were treated for 1h with either TG53 or MT-4 in serum-free media at 37°C, and then seeded onto FN-coated glass bottom microwell dishes (MatTek Corp. Ashland, MA) for 45 minutes at 37°C. Samples were fixed in PFA and blocked in 1% BSA. β1 integrin receptors were detected by using anti-β1 integrin antibodies (clone P5D2, Chemicon, #MAB1959, 1:100) and AlexaFluor 568-conjugated anti-mouse secondary antibodies, while actin was labeled using Alexa Fluor 488-conjugated phalloidin. Cells were imaged with a Nikon Ti2 Microscope equipped with a Photometrics Prime 95B camera using a Nikon Plan Apo 100× 1.49 NA TIRF objective.

In vivo cell attachment

All animal experiments were conducted in accordance with the recommendations for the Care and Use of Laboratory Animals of the National Institutes of Health under a protocol approved by Indiana University Institutional Animal Care and Use Committee. 5×10^6 SKOV3-GFP cells diluted in 100μl were injected intraperitoneally (ip) along with compound MT4 or MT6 (10μg/kg) in six-week-old female NOD-SCID gamma (NSG) mice (Jackson laboratories). After 2 hours, mice were euthanized, and the peritoneal cavity was washed thoroughly with 4 mL PBS. The peritoneal fluid containing cells that had not adhered to the mesothelial layer was gently collected and cell number was determined by using the Luna FL Cell Counter (Logos Biosystems). Ten replicates per group were assessed.

Enzyme-linked Immunosorbent Assay (ELISA); TG2 enzymatic activity assay; CCK-8 cell proliferation assays; Solid phase adhesion assay; Solubility assay, Wound-healing assay; Early attachment assay; Immunofluorescent (IF) staining and confocal microscopy; Western blotting; Colony and sphere forming assays, see Supplementary material (SM) and published methods (5, 13, 16).

Statistical analysis

GraphPad 7.04 Software (Prism, San Diego, CA, USA) was used for all statistical analyses. The Student's *t* test was used to test statistical significance between groups.

Results

Design and synthesis of new SMIs targeting TG2-FN interaction

Six new compounds were designed based on the chemical structure of the previously reported diaminopyrimidine derivative TG53 (13). The structure of **TG-53** is shown in Figure 1. Hit optimization strategy was focused on the improvement of **TG-53** potency and solubility. A small group of derivatives were designed to diversify the carboxylic amide

group of **TG-53** (Figure 1). Compounds **MT-3**, **MT-5**, and **MT-6** were designed to increase the binding activity by enhancing the potential interaction between the molecule and the target protein. **MT-3** adds an additional chloride group at the *p*-position; **MT-6** substitutes the original chlorine atom with a larger bromo group; and **MT-5** replaces the benzene ring with a larger naphthalene ring. Compounds **MT-1**, **MT-2** and **MT-4** were designed to increase the solubility. **MT-1** installs an amine group to replace the chloride, which should improve compound solubility under acidic conditions; **MT-2** uses a methoxyl group to replace the chloride, which should improve solubility at neutral pH; and **MT-4** adds an additional methylene group between the two aromatic groups (Figure 1), which increases the flexibility of the whole molecule, and thus should increase the overall solubility under all conditions. The measured solubility of MT4 was 91.5 μM compared to TG53 (< 5 μM; see SM).

In vitro inhibition of TG2/FN byMT1−6 compounds

The effects of MT1-MT6 on the interaction between rTG2 and FN42 were measured first by ELISA (13). MT-3, MT-4, MT-5, and MT-6 inhibited the interaction slightly more potently than TG53 at 10μM and similar to TG53 at 25 μM (Figure 2A). Next, BLI was employed to determine to kinetics of the TG2/FN interaction. As reported previously (17), TG2 and FN interact with high affinity. In our assay, the association and dissociation kinetics were: k_a=5320/Ms, k_d=0.0016/s (Figure 2B) and the equilibrium affinity (Kd) was 0.30nM. To examine the effect of MT4 on the formation of the rTG2-FN45 complex, first, FN45 was first captured on BLI sensors and incubated with MT4 in concentrations ranging from 16nM to 500μM for 15, 30, and 45 minutes. In these experiments, FN45 and rTG2 complex formation was not affected by MT4. Second, rTG2 was incubated with MT4, prior to BLI. Dose-dependent inhibition of the association between FN45 and rTG2 was observed (Figure 2C). The interaction decreased with increasing MT4 concentrations, and a faster dissociation was observed in the presence of MT4 (Figure 2D), suggesting that MT4 binds to TG2 and disrupts the binding interface with FN. To further examine this possibility, calorimetric titrations of MT4 into rTG2 were performed. The observed change in enthalpy for this interaction, H, was −20.5 kcal/mol and the apparent equilibrium dissociation constant, Kd, was 5.1 μM (Figure S7), supporting that MT4 interacts with TG2.

Next, the effects of TG53 and analogues on the enzymatic function of TG2 were measured by using a TGase colorimetric assay (18). The SMIs did not interfere with the enzymatic activity of TG2 (Figure S8), consistent with the fact that the enzymatic core of the protein (Cys[277]) is distinct from the FN-binding site (aa[88−106])(19).

Effects of MT1−6 on cell adhesion:

To measure whether disruption of the TG2-FN complex interferes with cellular adhesion to the ECM, a solid phase assay quantified OC cell attachment onto FN in the presence of SMIs or DMSO. MT2, MT4, MT5, and MT6 potently blocked OC cells' adhesion to FN (Figure 2E, *, $p<0.05$; **, $p<0.01$). Because MT-4 was active and the most soluble (see SM), we characterized its effects in-depth, as a representative of this series. Solid phase assays performed with SKOV3 (Figure 2F), OVCAR433 (Figure 2G) and OVCAR5 (Figure 2H)

demonstrated dose-dependent inhibitory effect of MT-4 on OC cell adhesion to FN. MT-4 was more active than TG53 at 10μM (**, p<0.01, Figure 2G–H).

SMIs prevent the formation of stable cell contacts with the FN

It has been proposed that TG2 facilitates formation of a "bridge" connecting integrin β1 with FN in the ECM (2). TG2/FN/integrin complexes are known to activate downstream signaling. Among the key proteins engaged after cell adhesion and spreading are the focal adhesion kinase (FAK) and the kinase c-Src, which is required for rapid actin and F-actin reorganization after early spreading (20). Therefore, we next investigated how inhibition of TG2-FN interaction by TG-53 and related inhibitors affects integrin clustering and downstream signaling, by using both immunofluorescent (IF) staining and western blotting.

First, the interaction between TG2 with proteins in the integrin β1 adhesion complex was measured by confocal IF analysis of SKOV3 cells, in the presence or absence of 1 μM TG53 (Figure 3A–D). A significant decrease in colocalization of TG2 with integrin β1 (Figure 3A), phosphorylated FAK (pFAK) (Figure 3B), c-Src (Figure 3C), and phosphorylated Src (pSrc) (Figure 3D) was recorded. Moreover, a marked decrease in FAK and Src phosphorylation was observed downstream of integrin β1 upon treatment with TG53 (Figures 3B and D).

Next, we sought to dissect the mechanism by which TG53 and related SMIs interfere with cell attachment. For this, we performed an *in vitro* early cell attachment assay using OVCAR5 cells pre-treated with TG53 or MT4 (1μM) for 72 hours. Cells were seeded for 30 minutes in serum-free media onto FN coated cover slips. IF staining for vinculin showed that exposure of cells to both MT-4 and TG53 before and during cell attachment decreased the number of focal contacts established with FN-coated substrate in comparison with DMSO treated controls (Figure 4A, upper panel). While the vehicle treated cells established maturing focal adhesions (elongated shape, Figure 4A, DMSO/DMSO, inset), cells treated with SMIs exhibited immature contacts (punctate shape, Figure 4A, TG53/TG53, MT-4/MT-4, insets). Increased vinculin staining around the nucleus as compared to cell periphery was observed in cells treated with MT4, suggesting a lack of productive engagement of cell protrusions to bind FN. Both TG-53 and MT4 caused decreased FAK phosphorylation (Figure 4A, bottom panel). Staining of actin filaments with phalloidin revealed generation of thin cell protrusions towards the FN surface in DMSO treated cells (Figure 4B, left panel). However, in cells pre-treated with MT-4, although these protrusions were formed, they could not establish durable connections with the FN substrate. As a consequence of mechanic tension, they snapped back forming curly ruffles (Figure 4B, middle panel, arrows). Also, cells lost polarity after exposure to MT-4 prior and during attachment, as evidenced by the formation of multiple lamellipodia (Figure 4B, right panel, arrows). The absence of a single leading-edge characteristic of directional cell migration is clearer in high-contrast grayscale images illustrating the actin cytoskeleton affected by MT-4 treatment (Figure 4C, right panel) versus TG53 (Figure 4C, left panel). MT-4 treated cells displayed cortical localization of actin filaments, as opposed to TG53-treated cells, where parallel intracellular actin filaments are still present. This provides evidence that MT-4 affects actin cytoskeleton

remodeling. Moreover, MT-4 affected cell-ECM adhesion, while the cell-cell interactions appear unaffected (Figure 4B, middle and right panel versus left panel, arrowheads).

Having observed these effects exerted by SMIs on cell adhesion and based on previous knowledge that cell surface TG2 promotes integrin clustering (21), we next evaluated how targeting TG2-FN interaction impacts integrins' organization at the interface with FN. TIRF microscopy, which allows high resolution scanning at the cell-glass substrate interface through an evanescent light wave effect (22, 23) demonstrated that β1 integrins distribute evenly after OVCAR5 cells' attachment to FN-coated substrate (Figure 4D, top panels; Figure S9). DMSO (control) did not affect this pattern. Actin formed dense symmetrically distributed filaments that support the cell shape during cellular adhesion (Figure 4D, lower panels; Figure S9). Pre-treatment with 1μM or 5μM TG53 caused modest displacement of integrin receptors towards the cell perimeter and a disorganization of the actin cytoskeleton that form shorter spikes instead of long stretched filaments. Noteworthy, pre-incubation of OVCAR5 cells with 1μM or 5μM MT-4 caused enhanced β1 integrin transposition towards the extreme edge of the cell concurrent with cortical positioning of actin fibers (Figure 4A–C; Figure S9).

As a control, we used flow cytometry (FACS) to measure β1 integrin on the surface of cells treated with the SMIs. FACS did not show significant downregulation of β1 integrin receptors at the plasma membrane in SKOV3 and OVCAR5 cells treated with serial concentrations of TG53 and MT4, as compared to vehicle treated cells (Figure S10). As controls, an anti-integrin β1 function blocking antibody significantly decreased β1 integrin expression, while a non-specific IgG control did not cause any changes. Altogether, TIRF and FACS analyses indicate that the main effect of the SMIs is redistribution of β1 integrin receptors towards the cortical region, with only minor changes observed at the plasma membrane (Figure 4D and S10).

SMIs attenuate signaling downstream of integrin β1

The effects of selected SMIs on "outside in" signaling activated in response to cell adhesion were also measured by Western blotting. Treatment of OC cells with TG53 (8 to 16 μM) attenuated FAK phosphorylation (Figure S11). Similarly, MT-4 and MT-5 caused dose-dependent inhibition of FAK phosphorylation (Figure S11). A time course experiment compared the effects of MT4 and of the parent compound TG53, on signaling activated in response to OVCAR5 cell attachment (Figure 5A). FAK phosphorylation was modestly delayed in the presence of TG53, with a peak in activation at 30 minutes post cell seeding on FN as compared to 15 minutes for control (Figure 5A, left). This inhibition was more evident after treatment with MT-4 (Figure 5A, right), consistent with the results of the IF analysis. ERK phosphorylation was also inhibited and delayed in cells treated with MT-4 as compared to control or TG53-treated cells (Figure 5A).

SMIs prevented attachment of OC cells to a mesothelial cell layer *in vitro* and to peritoneum *in vivo*

As cellular adhesion has a potential impact on OC metastasis (24), the new SMIs could be developed as inhibitors of peritoneal dissemination. Based on results of previous analyses,

MT4, MT5, and MT6 were selected for further characterization. First, cell adhesion to a mesothelial layer resembling the peritoneal cavity derived from LP9 normal primary mesothelial cells (25, 26) was assessed. Calcein-labeled OC cells were allowed to adhere to LP9 confluent monolayers in the presence of the SMIs or vehicle control. MT-4 and MT-5 significantly decreased SKOV3 cell binding to the mesothelial layer (Figure 5B, ***$p<0.001$, ****$p<0.0001$). MT4, MT5, MT6 exerted a dose-dependent inhibitory effect on OVCAR433 adhesion to the LP9 layer, at concentrations >10 μM (Figure 5C, **$p<0.01$, ***$p<0.001$).

After cell adhesion to the mesothelium, the next step in the process of peritoneal metastasis, is migration and invasion into the matrix. Thus, effects of SMIs on OC cell migration on FN coated substrates were also determined. MT4, MT5 and MT6 (8μM), inhibited the motility of SKOV3 and OVCAR5 cells as measured by the ability to repair a scratch produced in the monolayer (Figure 5D–E, **$p<0.01$, *** $p<0.001$, ****$p<0.0001$).

Lastly, the effects of SMIs on adhesion to the peritoneum were assessed *in vivo*. Stably expressing GFP SKOV3 cells pre-incubated with MT4 or MT-6 for 1 hour were injected ip. Two hours after injection, unattached cells were recovered from the peritoneal cavity and counted (Figure S12). Increased numbers of OC cells were recovered from mice injected with MT4 or MT6, as compared to vehicle (Figure 5F, G). MT-4 was more potent ($p<0.0001$) than MT-6 ($p<0.05$) preventing attachment of SKOV3 cells to the peritoneal cavity. These data support further development of this class of compounds to prevent peritoneal dissemination.

Anti-proliferative effects:

The parent compound TG53 was not cytotoxic (13). Similarly, the analogues MT1–6 did not exert anti-proliferative effects in SKOV3 cells during a 72-hour treatment period (Figure 6A–B). We next considered potential combinations of the proposed SMIs with cytotoxic drugs and tested whether the compounds potentiated the effects of paclitaxel (PTX). Priming with 1μM MT4 before PTX diminished colony formation compared to control (DMSO) or TG53-primed cells (Figure 6C–D). Similarly, the combination of MT-4 and PTX inhibited OVCAR5 cell proliferation as spheres more potently than PTX alone or PTX and TG53 (Figure 6E–F). However, priming of OVCAR-5 cells with TG2-FN inhibitors did not interfere with cell cycle progression (Figure S13A) or induced apoptosis as evidenced by Annexin V/7-AAD double staining (Figure S13B). These results support that priming of OC cells with TG2-FN inhibitors potentiate effects of PTX by interfering with cell attachment to the FN-rich ECM, without affecting cell viability or cell cycle progression.

Discussion

Our results provide data on newly developed SMIs targeting the interaction between TG2 and FN. We had previously reported TG53 as a lead inhibitor selected from high throughput screening of the ChemDiv library using an Alpha-Lisa assay (13). Here we characterize a series of analogues developed by using rational medicinal chemistry design and show that the analogues blocked TG2-FN interaction *in vitro* and OC cell adhesion to FN and to reconstituted peritoneal matrices *in vitro* and *in vivo*. Furthermore, the lead analogue, MT-4

prevented formation of stable focal contacts and mature focal adhesions to FN. Such compounds are predicted to block metastasis and to increase anoikis of unattached cells in the peritoneal cavity. These data have several implications.

First, we provide information on a new class of SMIs which block integrin-dependent adhesion and "outside-in signaling". We show that chemical optimization of the "hit" diaminopyrimidine compound **TG-53** was possible. The strategy aimed to improve potency and solubility of the hit compound by modifying its amide group. The derivative compounds demonstrated selective binding to TG2 and improved solubility (TG53< 5μM vs. MT-4; 91.5μM and MT-6; 6.4μM). While the proposed inhibitors demonstrate activity *in vitro* at low μM concentrations, in cellular and in vivo models, higher concentrations were required to attain the desired effects, suggesting that future chemical optimization of these compounds will be needed to improve their potency. Noteworthy, biophysical measurements using BLI and ITC revealed that MT-4 bound directly to TG2 and prevented its interaction with the FN 45 kDa fragment. This suggested that in the presence of the inhibitor, TG2 would be prevented from bridging integrin β1 and FN in the ECM, hindering cell adhesion to the matrix.

Confocal microscopy supported this assumption, as TG2 colocalization with integrin β1 and FN in the adhesion complexes was decreased by the SMIs. In the absence of a strong interaction with the matrix, integrin β1 was displaced from the cell cortex, as shown by TIRF microscopy. Consequently, OC cells formed loose, unstable focal adhesions, with cell displaying curly ruffles at the plasma membrane and loss of cell polarity due to decreased lamellipodia in the presence of the inhibitors. This translated in a dose-dependent decrease of OC cells attachment to FN upon pre-treatment with the SMIs, as measured by solid phase assays. As TG2 was previously shown to induce integrin clustering independent from integrin-ligand interaction (21) and we observed partial loss of integrins colocalization in the presence of the SMIs, we inferred that by disrupting the interaction of TG2 with FN, integrin translocation from adhesion contacts was prevented and formation of an FN matrix could be inhibited (27). By preventing the accumulation of fibrillar FN in the tumor ECM, these TG2-FN SMIs could have a long-term effect on tumor cells' attachment to peritoneal sites. Additionally, these inhibitors will permit an in-depth evaluation of molecular events linked to integrin-dependent cell adhesion in contexts other than cancer.

FN is one of the most abundant ECM proteins in omentum and peritoneum (28). Adhesion of OC cells to FN *via* α5β1 integrin activates "outside-in signaling" by inducing phosphorylation of FAK, either directly (29) or through c-Met (30). This leads to activation of both survival (AKT) and mitogenic (MAPK) pathways (31), supporting cell proliferation and tumor growth (32). The β1 integrin-FN complex is strengthened by interactions with TG2, a protein we discovered to be overexpressed in OC (33). Here we show that inhibition of the TG2/FN complex by the new SMIs also delays and attenuates activation of FAK in response to cell adhesion. We had previously demonstrated the significance of TG2 to peritoneal dissemination through a β1 integrin dependent mechanism (3), as well as the significance of the TG2/FN/integrin complex to the survival of OC stem cells (5). Our current results using SMIs are consistent with our previous observations showing that targeting this complex, by using a function blocking antibody against the FN-binding

domain of TG2 decreased spheroid proliferation and tumor initiation capacity (34). Together, these data support that the TG2/FN complex is an important cancer target.

Second, we provide here the first *in vivo* evidence on the potential of TG2-FN inhibitors to interfere with peritoneal metastasis. SKOV3 cells that were pretreated with either MT-4 or MT-6 before injection in the peritoneal cavity of immunodeficient mice, attached less efficiently to the peritoneal walls, as illustrated by the increased recovery of these cells 2 hours after inoculation. These findings were also corroborated by the solid phase assays performed by using LP9 cells, as a model of the peritoneal mesothelial lining, which showed that fewer cells attached to the mesothelial monolayer in the presence of the SMIs.

Similar cell-adhesion blocking strategies under development include the use of function-inhibiting antibodies against integrin receptors or against the hyaluronan receptor, CD44. These agents were shown to prevent the attachment of OC cells to the mesothelial monolayer (35–37). As $\alpha5\beta1$ integrin is expressed on both OC tumor cells as well as on endothelial cells (38), targeting this heterodimer was expected to interfere with tumor growth and dissemination in solid tumors, including in OC (30). Although promising in preclinical models, anti-integrin antibodies have not yet demonstrated clinical benefit in patients with advanced stage solid tumors (39). This could be due to their initial testing in late stages of the disease, after metastases had been established. Future refinement of this strategy targeting adhesion to the peritoneum warrants further investigation, in settings preceding wide-spread tumor dissemination or in combination with standard cytotoxic therapy.

Third, we show that priming of OC cells with TG2/FN inhibitors, sensitized cells to paclitaxel. A potential mechanism underlying this interaction may be related to inhibition of "outside-in signaling", which provides survival signals. We and others have previously shown that TG2 knock down increased response to chemotherapy in breast, ovarian and pancreatic cancer (12, 40–42), but this is the first demonstration that inhibition of the interaction with FN sensitizes cancer cells to chemotherapy. This concept deserves further exploration along with future testing of potential synergistic combinations with other cytotoxic or biological anti-cancer agents. In all, our results support further development of TG2/FN blockade as a new strategy to inhibit peritoneal metastasis and/or to sensitize cancer cells to standard cytotoxic therapy. Further medicinal chemistry-based optimization of this class of compounds is necessary to improve their properties and bioavailability *in vivo*.

Supplementary Material

Refer to Web version on PubMed Central for supplementary material.

Acknowledgments:

References

1. Naora H, Montell DJ. Ovarian cancer metastasis: integrating insights from disparate model organisms. Nat Rev Cancer. 2005;5(5):355–66. [PubMed: 15864277]

2. Akimov SS, Krylov D, Fleischman LF, Belkin AM. Tissue transglutaminase is an integrin-binding adhesion coreceptor for fibronectin. J Cell Biol. 2000;148(4):825–38. [PubMed: 10684262]

3. Satpathy M, Cao L, Pincheira R, Emerson R, Bigsby R, Nakshatri H, et al. Enhanced peritoneal ovarian tumor dissemination by tissue transglutaminase. Cancer Res. 2007;67(15):7194–202. [PubMed: 17671187]

4. Shao M, Cao L, Shen C, Satpathy M, Chelladurai B, Bigsby RM, et al. Epithelial-to-mesenchymal transition and ovarian tumor progression induced by tissue transglutaminase. Cancer Res. 2009;69(24):9192–201. [PubMed: 19951993]

5. Condello S, Sima LE, Ivan C, Cardenas H, Schiltz GE, Mishra RK, et al. Tissue transglutaminase regulates interactions between ovarian cancer stem cells and the tumor niche. Cancer Res. 2018.

6. Steeg PS. Tumor metastasis: mechanistic insights and clinical challenges. Nat Med. 2006;12(8): 895–904. [PubMed: 16892035]

7. Buczek-Thomas JA, Chen N, Hasan T. Integrin-mediated adhesion and signalling in ovarian cancer cells. Cell Signal. 1998;10(1):55–63. [PubMed: 9502118]

8. Cao L, Shao M, Schilder J, Guise T, Mohammad KS, Matei D. Tissue transglutaminase links TGF-beta, epithelial to mesenchymal transition and a stem cell phenotype in ovarian cancer. Oncogene. 2012;31(20):2521–34. [PubMed: 21963846]

9. Satpathy M, Shao M, Emerson R, Donner DB, Matei D. Tissue transglutaminase regulates matrix metalloproteinase-2 in ovarian cancer by modulating cAMP-response element-binding protein activity. The Journal of biological chemistry. 2009;284(23):15390–9. [PubMed: 19324884]

10. Condello S, Cao L, Matei D. Tissue transglutaminase regulates beta-catenin signaling through a c-Src-dependent mechanism. FASEB journal : official publication of the Federation of American Societies for Experimental Biology. 2013.

11. Yakubov B, Chelladurai B, Schmitt J, Emerson R, Turchi JJ, Matei D. Extracellular tissue transglutaminase activates noncanonical NF-kappaB signaling and promotes metastasis in ovarian cancer. Neoplasia. 2013;15(6):609–19. [PubMed: 23730209]

12. Cao L, Petrusca DN, Satpathy M, Nakshatri H, Petrache I, Matei D. Tissue transglutaminase protects epithelial ovarian cancer cells from cisplatin-induced apoptosis by promoting cell survival signaling. Carcinogenesis. 2008;29(10):1893–900. [PubMed: 18667446]

13. Yakubov B, Chen L, Belkin AM, Zhang S, Chelladurai B, Zhang ZY, et al. Small molecule inhibitors target the tissue transglutaminase and fibronectin interaction. PLoS One. 2014;9(2):e89285. [PubMed: 24586660]

14. Shah NB, Duncan TM. Bio-layer interferometry for measuring kinetics of protein-protein interactions and allosteric ligand effects. J Vis Exp. 2014(84):e51383. [PubMed: 24638157]

15. Wartchow CA, Podlaski F, Li S, Rowan K, Zhang X, Mark D, et al. Biosensor-based small molecule fragment screening with biolayer interferometry. J Comput Aided Mol Des. 2011;25(7): 669–76. [PubMed: 21660516]

16. Condello S, Cao L, Matei D. Tissue transglutaminase regulates beta-catenin signaling through a c-Src-dependent mechanism. FASEB J. 2013;27(8):3100–12. [PubMed: 23640056]

17. Cardoso I, Osterlund EC, Stamnaes J, Iversen R, Andersen JT, Jorgensen TJ, et al. Dissecting the interaction between transglutaminase 2 and fibronectin. Amino Acids. 2017;49(3):489–500. [PubMed: 27394141]

18. Folk JE, Cole PW. Mechanism of action of guinea pig liver transglutaminase. I. Purification and properties of the enzyme: identification of a functional cysteine essential for activity. J Biol Chem. 1966;241(23):5518–25. [PubMed: 5928192]

19. Hang J, Zemskov EA, Lorand L, Belkin AM. Identification of a novel recognition sequence for fibronectin within the NH2-terminal beta-sandwich domain of tissue transglutaminase. J Biol Chem. 2005;280(25):23675–83. [PubMed: 15849356]

20. Partridge MA, Marcantonio EE. Initiation of attachment and generation of mature focal adhesions by integrin-containing filopodia in cell spreading. Mol Biol Cell. 2006;17(10):4237–48. [PubMed: 16855018]

21. Janiak A, Zemskov EA, Belkin AM. Cell surface transglutaminase promotes RhoA activation via integrin clustering and suppression of the Src-p190RhoGAP signaling pathway. Mol Biol Cell. 2006;17(4):1606–19. [PubMed: 16452636]

22. Poulter NS, Pitkeathly WT, Smith PJ, Rappoport JZ. The physical basis of total internal reflection fluorescence (TIRF) microscopy and its cellular applications. Methods Mol Biol. 2015;1251:1–23. [PubMed: 25391791]

23. Worth DC, Parsons M. Advances in imaging cell-matrix adhesions. J Cell Sci. 2010;123(Pt 21): 3629–38. [PubMed: 20971702]

24. Bast RC Jr., Hennessy B, Mills GB. The biology of ovarian cancer: new opportunities for translation. Nat Rev Cancer. 2009;9(6):415–28. [PubMed: 19461667]

25. Kenny HA, Nieman KM, Mitra AK, Lengyel E. The first line of intra-abdominal metastatic attack: breaching the mesothelial cell layer. Cancer Discov. 2011;1(2):100–2. [PubMed: 22013555]

26. Kenny HA, Dogan S, Zillhardt M, KM A, Yamada SD, Krausz T, et al. Organotypic models of metastasis: A three-dimensional culture mimicking the human peritoneum and omentum for the study of the early steps of ovarian cancer metastasis. Cancer Treat Res. 2009;149:335–51. [PubMed: 19763444]

27. Clark K, Pankov R, Travis MA, Askari JA, Mould AP, Craig SE, et al. A specific alpha5beta1-integrin conformation promotes directional integrin translocation and fibronectin matrix formation. J Cell Sci. 2005;118(Pt 2):291–300. [PubMed: 15615773]

28. Kenny HA, Lengyel E. MMP-2 functions as an early response protein in ovarian cancer metastasis. Cell Cycle. 2009;8(5):683–8. [PubMed: 19221481]

29. Schlaepfer DD, Jones KC, Hunter T. Multiple Grb2-mediated integrin-stimulated signaling pathways to ERK2/mitogen-activated protein kinase: summation of both c-Src- and focal adhesion kinase-initiated tyrosine phosphorylation events. Mol Cell Biol. 1998;18(5):2571–85. [PubMed: 9566877]

30. Mitra AK, Sawada K, Tiwari P, Mui K, Gwin K, Lengyel E. Ligand-independent activation of c-Met by fibronectin and alpha(5)beta(1)-integrin regulates ovarian cancer invasion and metastasis. Oncogene. 2011;30(13):1566–76. [PubMed: 21119598]

31. Renshaw MW, Price LS, Schwartz MA. Focal adhesion kinase mediates the integrin signaling requirement for growth factor activation of MAP kinase. J Cell Biol. 1999;147(3):611–8. [PubMed: 10545504]

32. Ward KK, Tancioni I, Lawson C, Miller NL, Jean C, Chen XL, et al. Inhibition of focal adhesion kinase (FAK) activity prevents anchorage-independent ovarian carcinoma cell growth and tumor progression. Clin Exp Metastasis. 2013;30(5):579–94. [PubMed: 23275034]

33. Matei D, Graeber TG, Baldwin RL, Karlan BY, Rao J, Chang DD. Gene expression in epithelial ovarian carcinoma. Oncogene. 2002;21(41):6289–98. [PubMed: 12214269]

34. Condello S, Sima L, Ivan C, Cardenas H, Schiltz G, Mishra RK, et al. Tissue Tranglutaminase Regulates Interactions between Ovarian Cancer Stem Cells and the Tumor Niche. Cancer Res. 2018;78(11):2990–3001. [PubMed: 29510995]

35. Strobel T, Cannistra SA. Beta1-integrins partly mediate binding of ovarian cancer cells to peritoneal mesothelium in vitro. Gynecol Oncol. 1999;73(3):362–7. [PubMed: 10366461]

36. Cannistra SA, Kansas GS, Niloff J, DeFranzo B, Kim Y, Ottensmeier C. Binding of ovarian cancer cells to peritoneal mesothelium in vitro is partly mediated by CD44H. Cancer Res. 1993;53(16): 3830–8. [PubMed: 8339295]

37. Strobel T, Swanson L, Cannistra SA. In vivo inhibition of CD44 limits intra-abdominal spread of a human ovarian cancer xenograft in nude mice: a novel role for CD44 in the process of peritoneal implantation. Cancer Res. 1997;57(7):1228–32. [PubMed: 9102203]

38. Slack-Davis JK, Atkins KA, Harrer C, Hershey ED, Conaway M. Vascular cell adhesion molecule-1 is a regulator of ovarian cancer peritoneal metastasis. Cancer Res. 2009;69(4):1469–76. [PubMed: 19208843]

39. Raab-Westphal S, Marshall JF, Goodman SL. Integrins as Therapeutic Targets: Successes and Cancers. Cancers (Basel). 2017;9(9).

40. Verma A, Guha S, Diagaradjane P, Kunnumakkara AB, Sanguino AM, Lopez-Berestein G, et al. Therapeutic significance of elevated tissue transglutaminase expression in pancreatic cancer. Clin Cancer Res. 2008;14(8):2476–83. [PubMed: 18413840]

41. Verma A, Guha S, Wang H, Fok JY, Koul D, Abbruzzese J, et al. Tissue transglutaminase regulates focal adhesion kinase/AKT activation by modulating PTEN expression in pancreatic cancer cells. Clin Cancer Res. 2008;14(7):1997–2005. [PubMed: 18381937]

42. Verma A, Mehta K. Tissue transglutaminase-mediated chemoresistance in cancer cells. Drug Resist Updat. 2007;10(4–5):144–51. [PubMed: 17662645]
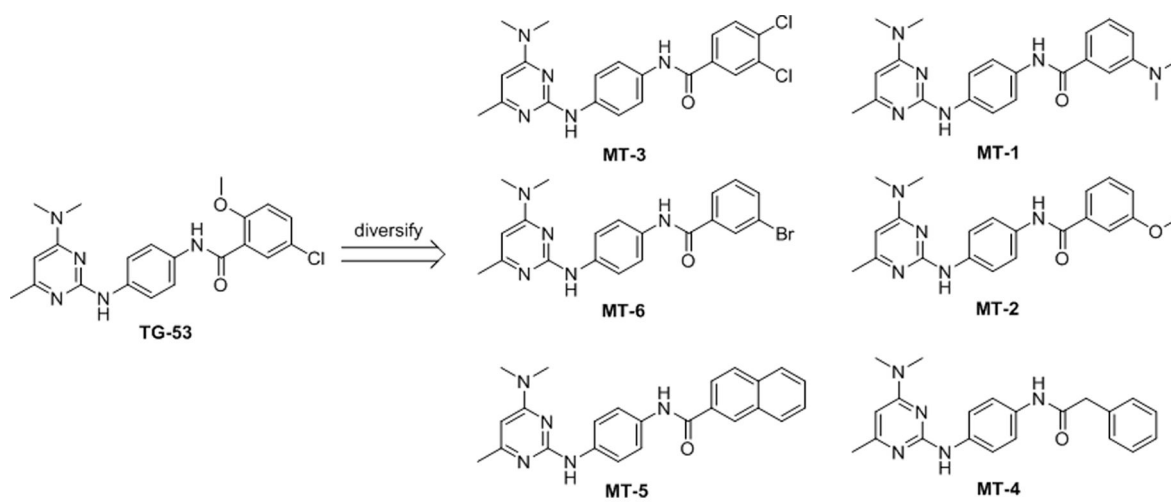
Figure 1. Chemical structures

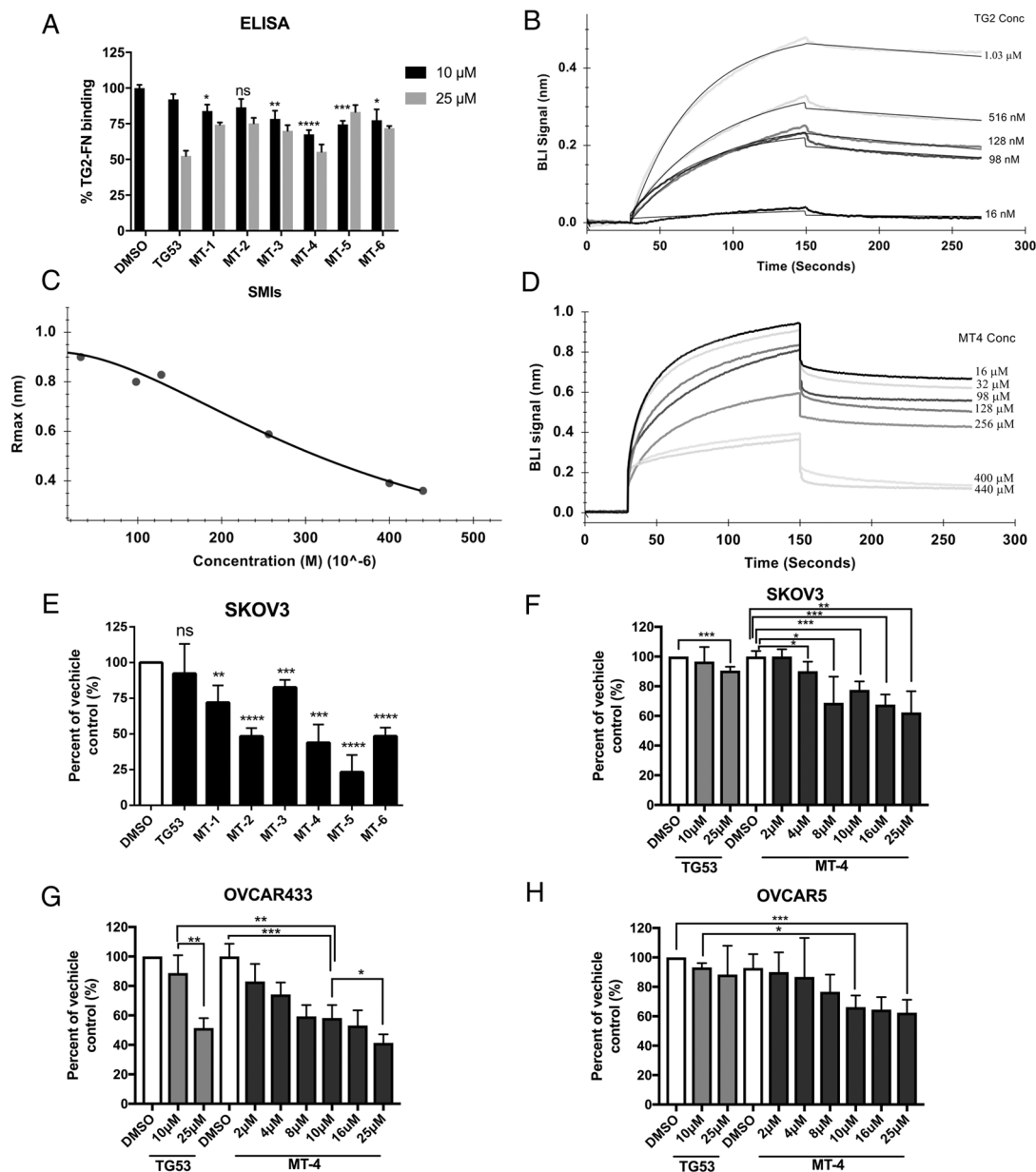of TG53 (parent compound) and of the 6 derivatives targeting the TG2-FN protein-protein interaction (MT1-MT6).

Figure 2. TG53 derivatives inhibit TG2-FN interaction.

A, ELISA measured the interaction between His-tagged TG2 and biotinylated FN42 in the presence of vehicle (DMSO, control), TG53 and MT1-MT6 at 10μM and 25μM concentrations. Bars represent means ± SD (n=3). **B**, Bio-layer Interferometry (BLI) sensograms monitor the real time association and dissociation kinetics of FN45 (captured on streptavidin-coated sensors) and TG2. The TG2 concentrations used at the association step are indicated. The nonlinear regression fits from 1:1 global analysis are shown as thin black lines; $k_a = 5320 \text{ M}^{-1}\text{s}^{-1}$ (±0.2%), $k_d = 0.0016 \text{ s}^{-1}$ (±0.4%), yielding $K_D = 0.30$ nM; goodness of fit: $R^2 = 0.996084$. **C**, Concentration-dependent inhibitory effect of MT4 on the FN45-TG2 interaction. For each MT4 concentration tested, the extent of binding (Rmax) was corrected for nonspecific binding of (TG2+MT4) to bare sensors. **D**, Bio-layer

Interferometry (BLI) sensograms show the real time association and dissociation kinetics of FN45 (20 μg/ml captured on streptavidin-coated sensors) and 1 μM TG2 pre-incubated with MT4 at various concentrations. **E**, Solid phase assay measured SKOV3 cells' adhesion to FN (5μg/mL) in the presence of TG53 and MT1–6 (n = 4). **F-H**, Dose-dependent effect of MT4 (2μM-25μM) on SKOV3 (**F**), OVCAR433 (**G**), and OVCAR5 (**H**) cells adhesion onto FN-coated plates was measured by a solid phase assay (see SM). For all experiments, results represent the mean and SD of at least triplicate samples: *p<0.05, **p<0.01, ***p<0.001, ****p<0.0001.
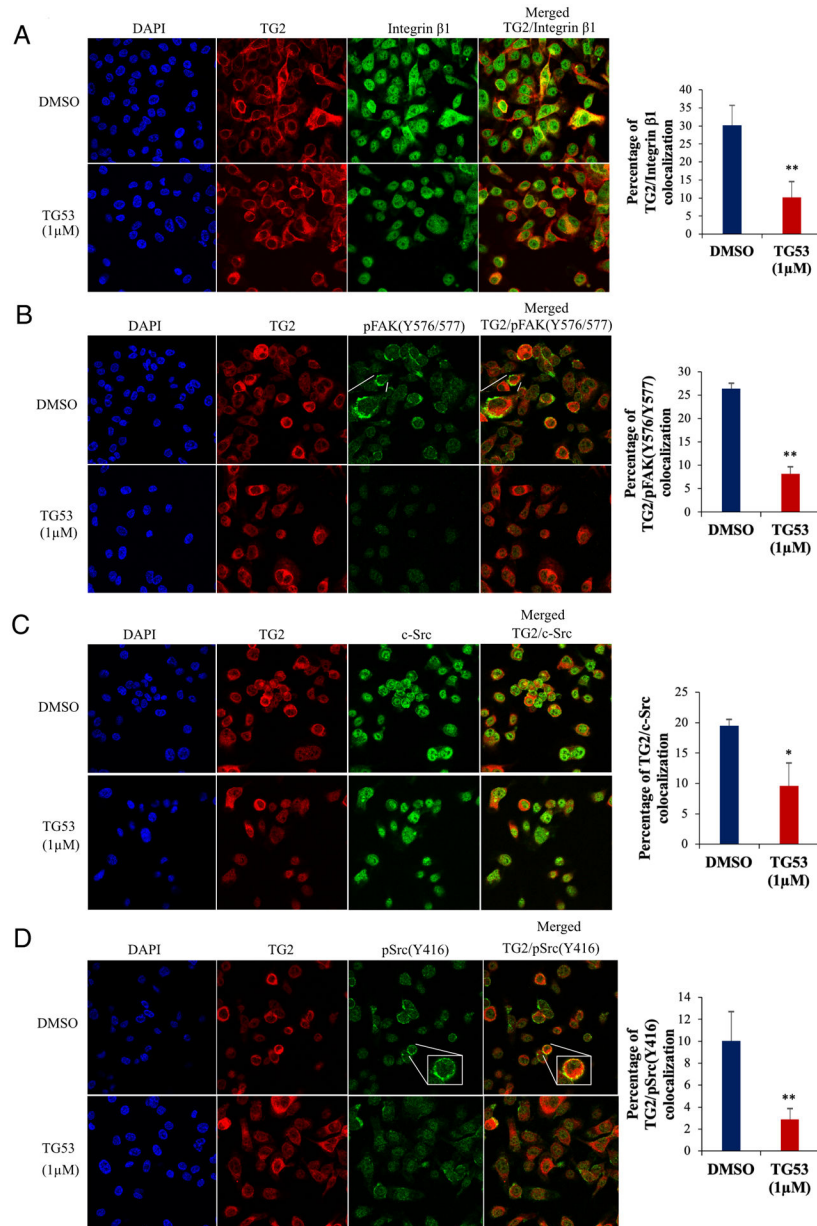
Figure 3. TG53 inhibits formation of a complex with integrin β1 and activation of FAK and c-Src during SKOV3 cell attachment onto FN.
A–D, Confocal microscopy analysis of TG2 (Cy5, red; ×600) co-localization with integrin β1, p-FAK (Y576/577), c-Src, and p-c-Src (Y416) (Alexa Fluor 488, green) in the presence of either 1μM TG53 (lower panels) or DMSO vehicle (upper panels). Graphs quantifying co-localization of the two proteins are presented. *p<0.05, **p<0.01.
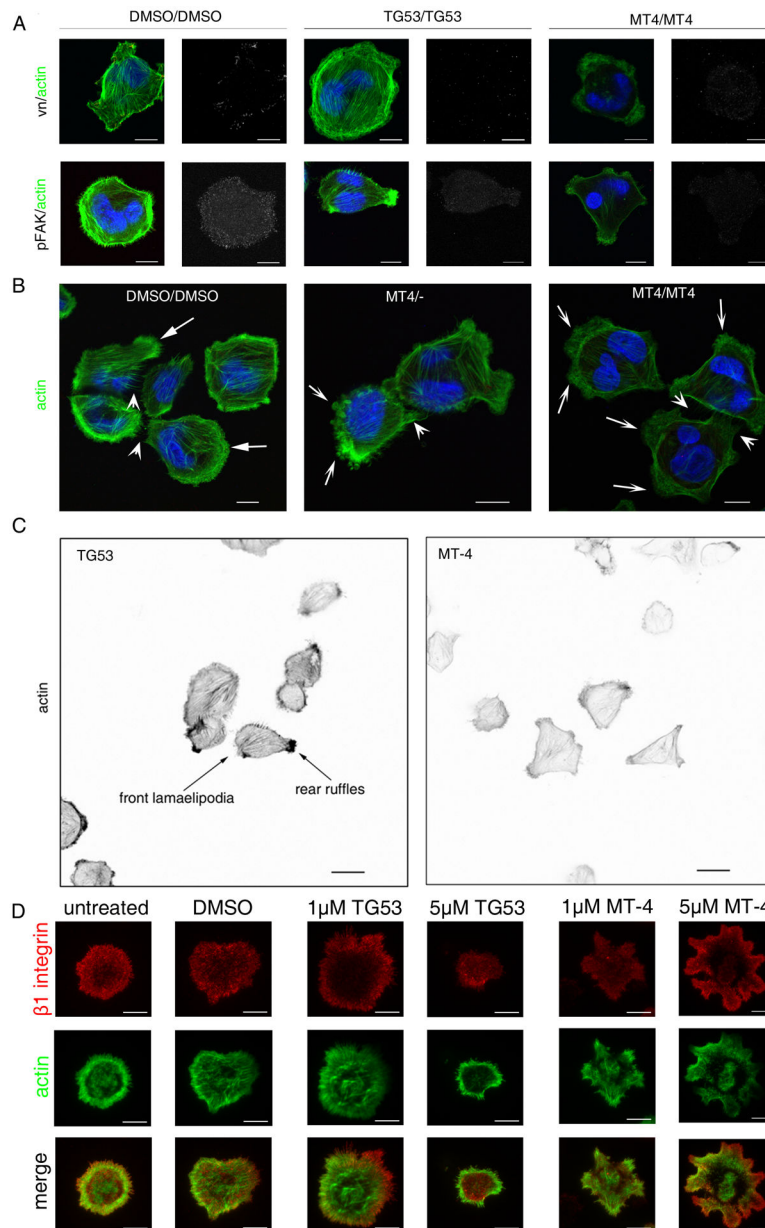
Figure 4. MT-4 inhibits early OVCAR5 cell attachment onto FN by interfering with the formation of stable focal contacts.

A–C, IF staining of adhesion complex factors in OVCAR5 cells upon cell adhesion to FN. **A**, Confocal imaging of intracellular localization of vinculin-positive focal adhesion points (white, upper panel), pFAK (white, lower panel), and actin filaments (green, upper and lower panel) at 30 minutes after seeding of OVCAR5 cells onto FN coated chamber slides in the presence or absence of inhibitors (TG53 and MT-4 at **1μM concentration**) or vehicle (DMSO). Cells were treated with the SMIs for 72 hours prior to seeding and during the assay. Insets provide detailed view of the vinculin-positive structures. Scale bar=10μm. **B**, Analysis of the actin cytoskeleton assessed morphological differences during cell attachment. Scale bar=10μm. **C**, Grayscale images of actin cytoskeleton in TG53- (left) and MT4- treated cells (right). Scale bar=20μm. **D**, TIRF microscopy analysis of OVCAR5 cells

pre-treated with SMIs for 1h to determine the distribution of integrin β1 (red, upper panels) at the interface with FN during cell attachment. Actin cytoskeleton is depicted in green (lower panels). Scale bar=10μm.

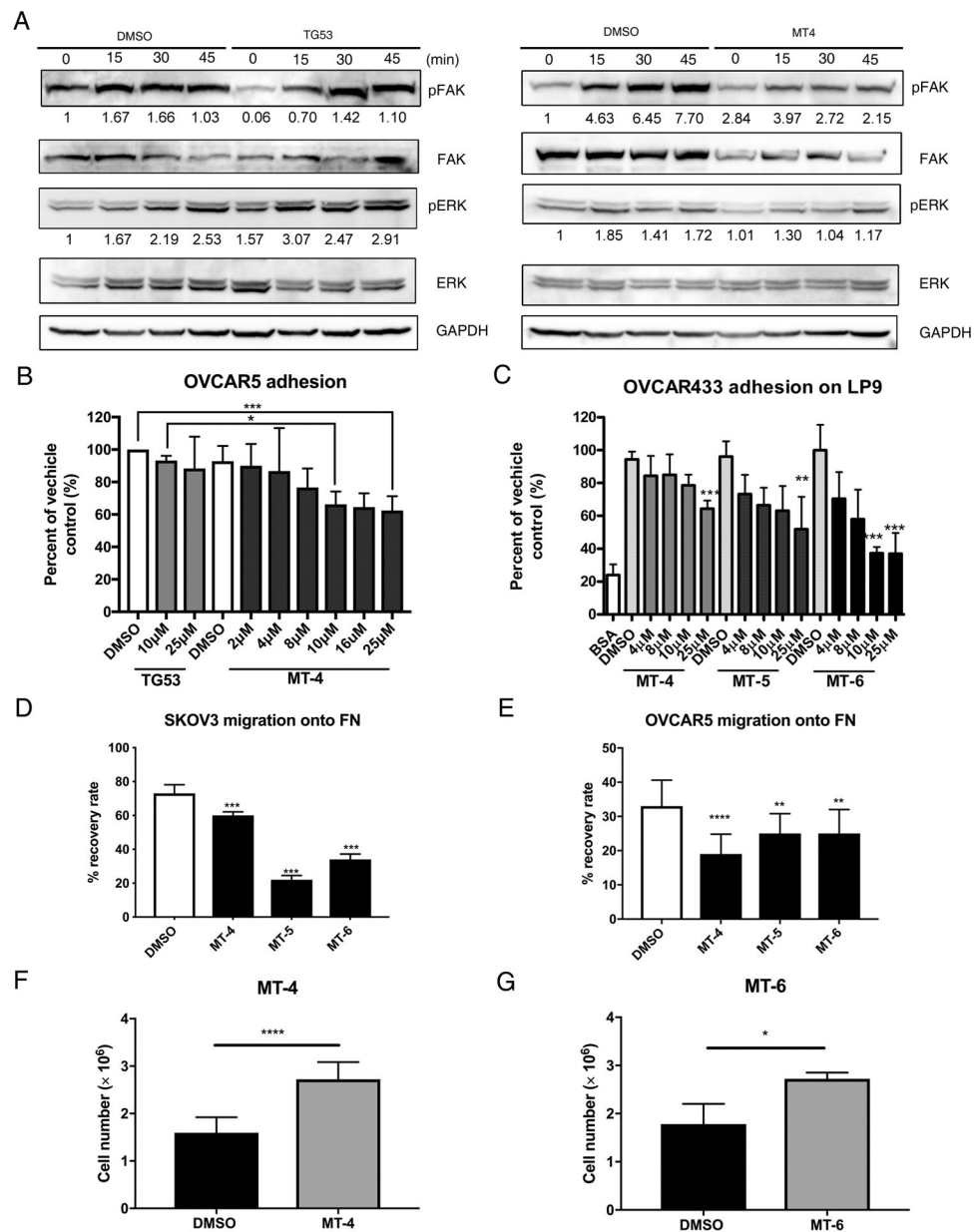**Figure 5. Effects of SMIs targeting the TG2/FN complex on "outside-in" signaling and adhesion to mesothelial surfaces.**

A, Western blot analysis of total and phosphorylated FAK and ERK was performed using cell lysates extracted from OVCAR cells plated on FN for 15 to 45 minutes in the presence of TG53 (left) or MT-4 (right) at 5μM concentration, as compared to DMSO. GAPDH was used as a control. OVCAR5 cells had been pretreated with the inhibitors for 72 hours. Densitometry analysis used the Quantity One software and results were normalized to GAPDH loading controls. DMSO 0 min time point was considered as 1 for comparative analysis. Values are shown for each band. **B**, A modified cell adhesion assay measured the effects of TG53, MT-4, MT-5, and MT-6 (25μM) on SKOV3 cells' adhesion onto semi-confluent LP9 monolayers. **C**, Dose-dependent effects of TG53, MT-4, MT-5, and MT-6 on OVCAR433 cells adhesion onto semi-confluent LP9 monolayers. **D–E**, Wound healing

assay measures migration of SKOV3 and OVCAR5 cells in the presence of MT-4, MT-5, MT-6 at a concentration of 8 μM (black bars) or vehicle (open bar). Migration rate was determined over a period of 24 hours by measuring the average distance between the wound borders at the beginning and at the end of the assay interval (n=4). **F**–**G**, SKOV3-GFP OC cells were injected ip in NSG mice in the presence of either MT-4 (10μg/kg) (**F**) or MT-6 (10μg/kg) (**G**) and allowed to attach to the peritoneal wall. After 2 hours, the cell suspension was recovered from the peritoneal cavity through peritoneal washings and the non-attached OC cells recovered were counted. *$p<0.05$, **$p<0.01$, ***$p<0.001$, ****$p<0.0001$.
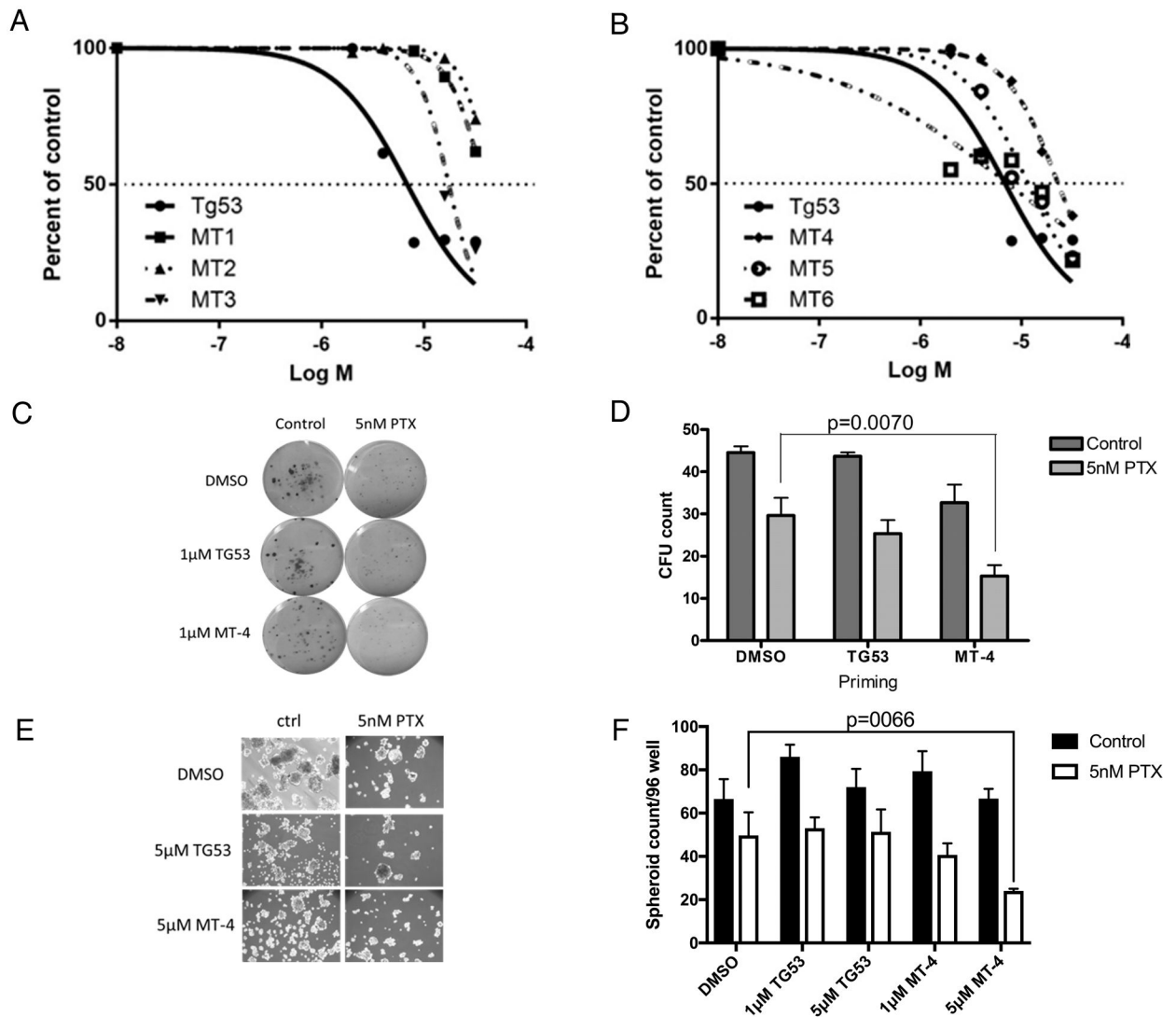
Figure 6. Priming of OVCAR5 cells with MT-4 sensitizes cells to paclitaxel (PTX).
A–B, The CCK8 assay was used to measure cell viability of SKOV3 cells treated with increasing concentrations of TG53 and MT1–6 for 72 hours. **C–D**, Colony formation from OVCAR-5 cells pre-treated with 1μM MT-4 or 1μM TG53 for 72 hours before seeding in the presence or absence of 5nM PTX (n=6; 10 days incubation to allow colonies formation). Colonies were stained with 0.4% crystal violet and counted using ImageJ. **E–F**, Sphere formation assay measured proliferation of OVCAR-5 cells pre-treated with 1μM MT-4 or 1μM TG53. Cells were allowed to form spheroids in the presence or absence of 5nM PTX (n = 3). Spheres were counted after ten days. *p<0.05, **p<0.01, ***p<0.001, ****p<0.0001.